Journal of Zhejiang University-SCIENCE B (Biomedicine & Biotechnology) 2023 24(6):510-523
www.jzus.zju.edu.cn; www.springer.com/journal/11585
E-mail: jzus_b@zju.edu.cn

Research Article

https://doi.org/10.1631/jzus.B2200447

Nanosilver alleviates foreign body reaction and facilitates wound repair by regulating macrophage polarization

Chuangang YOU[1*], Zhikang ZHU[1*], Shuangshuang WANG[1,2], Xingang WANG[1], Chunmao HAN[1✉], Huawei SHAO[1✉]

[1]*Department of Burns & Wound Care Center, the Second Affiliated Hospital, Zhejiang University School of Medicine, Hangzhou 310009, China*
[2]*Department of Burns, the First People's Hospital of Wenling, Wenling 317500, China*

Abstract: Foreign body reactions induced by macrophages often cause delay or failure of wound healing in the application of tissue engineering scaffolds. This study explores the application of nanosilver (NAg) to reduce foreign body reactions during scaffold transplantation. An NAg hybrid collagen-chitosan scaffold (NAg-CCS) was prepared using the freeze-drying method. The NAg-CCS was implanted on the back of rats to evaluate the effects on foreign body reactions. Skin tissue samples were collected for histological and immunological evaluation at variable intervals. Miniature pigs were used to assess the effects of NAg on skin wound healing. The wounds were photographed, and tissue samples were collected for molecular biological analysis at different time points post-transplantation. NAg-CCS has a porous structure and the results showed that it could release NAg constantly for two weeks. The NAg-CCS group rarely developed a foreign body reaction, while the blank-CCS group showed granulomas or necrosis in the subcutaneous grafting experiment. Both matrix metalloproteinase-1 (MMP-1) and tissue inhibitor of metalloproteinase-1 (TIMP-1) were reduced significantly in the NAg-CCS group. The NAg-CCS group had higher interleukin (IL)-10 and lower IL-6 than the blank CCS group. In the wound healing study, M1 macrophage activation and inflammatory-related proteins (inducible nitric oxide synthase (iNOS), IL-6, and interferon-γ (IFN-γ)) were inhibited by NAg. In contrast, M2 macrophage activation and proinflammatory proteins (arginase-1, major histocompatibility complex-II (MHC-II), and found in inflammatory zone-1 (FIZZ-1)) were promoted, and this was responsible for suppressing the foreign body responses and accelerating wound healing. In conclusion, dermal scaffolds containing NAg suppressed the foreign body reaction by regulating macrophages and the expression of inflammatory cytokines, thereby promoting wound healing.

Key words: Nanosilver; Macrophages; Implants; Foreign body reaction; Wound repair

1 Introduction

Wound healing of burns and trauma is compromised by various unfavorable factors, the most common of which are wound infection and an abnormal inflammatory response (Shi et al., 2020; Yang et al., 2021). Inflammation, as an important component present throughout the whole period of wound repair, plays a dominant role in necrosis elimination, pathogen suppression, and regulation of the immune microenvironment (Bergan, 2005; Forbes and Cooper, 2013; Wicks et al., 2014). Recently, tissue engineering products have been widely used for wound repair and skin regeneration. However, as foreign bodies, successful implantations of these products should overcome two obstacles: infection and foreign body reactions (Weng et al., 2020). Macrophages and giant cells will be activated and initiated to accumulate when medical devices, prostheses, or biomaterials are implanted (Sheikh et al., 2015). Inflammatory cells aggregate around the implant and absorb the proteins adhered to the surface, and macrophages become giant cells after they phagocytose and engulf the xenogenous ingredients and cellular debris (Anderson et al., 2008; O'Shea et al., 2020). Foreign body reactions conducted by macrophages often lead to local granulomatosis, which not only affects the lifespan of the implants but also causes delay or even

✉ Huawei SHAO, 2504131@zju.edu.cn
Chunmao HAN, zrssk@zju.edu.cn
* The two authors contributed equally to this work
Huawei SHAO, https://orcid.org/0000-0003-0310-9709
Chunmao HAN, https://orcid.org/0000-0002-2821-1323

Received Sept. 8, 2022; Revision accepted Jan. 27, 2023;
Crosschecked Apr. 27, 2023

suspension of the wound repair process (Anderson et al., 2008; Sheikh et al., 2015; Chiang et al., 2017).

In the process of wound repair, two types of macrophages are sequentially activated. As a scavenger, M1 macrophages participate in antiinfection and the formation of foreign-body giant cells at the early stage, whereas M2 macrophages are involved mainly in the middle stage of wound repair. The leading protagonist involved in the foreign body reaction is classically activated M1 macrophages (O'Shea et al., 2020). These M1-type macrophages gradually fuse with the implants and develop into foreign-body giant cells following the initiation of phagocytosis (Sheikh et al., 2015; Anderson and Jiang, 2017). Mast cells also recruit macrophages through degranulation and histamine secretion, contributing to the development of the foreign body reaction (Anderson et al., 2008; Shi et al., 2018; Villarreal-Leal et al., 2021). As a result, uncontrolled infection or inflammation at the early stage of implantation may lead to foreign body reactions and granuloma formation, which suppresses the physiological process of skin wound healing (Huang et al., 2018; Benayahu et al., 2020).

Our previous studies demonstrated that nanosilver (NAg)-loaded collagen-chitosan scaffold (NAg-CCS) was favorable and applicable for treating burn wounds. Apart from their antimicrobial effects, NAg-loaded scaffolds can also inhibit the abnormal inflammatory response effectively (You et al., 2012, 2017), though the mechanisms are still not fully understood. Therefore, we hypothesize that NAg might restrain the inflammatory response dominated by M1 macrophages and reduce the foreign body reaction induced by the implanted scaffolds, thereby accelerating tissue regeneration in situ. In this study, we constructed an NAg-CCS and applied it to a rat model by subcutaneous grafting and to a miniature pig model with skin wounds to explore the effects and mechanisms of action of NAg on inflammation and the foreign body reaction, using a set of pathological and biochemical experiments.

2 Materials and methods

2.1 Preparation of NAg-CCS

NAg-CCSs were prepared following the methods described previously (You et al., 2017). In brief, a collagen-chitosan mixture with NAg was prepared by dissolving type I collagen and chitosan (degree of deacetylation: ⩾85%; viscosity-average molecular weight (M_η): 1.06×10^5–1.71×10^5) in 0.5 mol/L acetic acid solution at a mass ratio of 9:1, followed by adding NAg solution and mixing thoroughly. The mixed solution was added to a 12-well plate (2 mL/well). Then the plate was incubated at 4 ℃ overnight, frozen at −20 ℃ for 2 h, and freeze-dried at −80 ℃ for 24 h to obtain the porous NAg-CCS. The freeze-dried NAg-CCSs were cross-linked in 20.6 mg/mL 1-ethyl-3-(3-dimethylaminopropyl)-carbodiimide/*N*-hydroxysuccinimide (EDC/NHS) solution for 24 h and subsequently rinsed with deionized water six times (10 min each) before secondary freeze-drying to obtain the cross-linked NAg-CCS. After drying, the NAg-CCS was examined under a scanning electronic microscope (Hitachi S-4800, Japan). NAg was purchased from Shanghai Huzhen Nanotechnology (Shanghai, China); Type I collagen was donated by Zhende Medical (Shaoxing, China); and acetic acid, EDC, and NHS were purchased from Sigma-Aldrich (St. Louis, USA). Before the animal experiments, all the scaffolds used in this study were sterilized by ultraviolet irradiation (both sides, for 30 min each) and soaked in phosphate-buffered saline (PBS; Solarbio Science and Technology, Beijing, China).

2.2 Release study and degradation study in vitro

In the release experiment, NAg-CCSs were immersed in PBS containing 25 U/mL collagenases (Solarbio Science and Technology) and incubated on a shaker in a 37 ℃ incubator (blank CCS with equivalent NAg solution as the control). Every 24 h, 300 μL of supernatant was collected and centrifuged in the Heraeus Multifuge X3R centrifuge (Thermo Fisher Scientific, Waltham, MA, USA) to remove the impurities. After collection, 300 μL collagenase-containing PBS solution was supplemented to maintain the release solution at a constant volume. On Day 15, 50 U of collagenase was added to completely degrade the scaffolds. The NAg content was detected by an inductively coupled plasma mass spectrometry system (ELAN DRC-e system, PerkinElmer, Waltham, MA, USA).

In the degradation experiment, scaffolds (n=3 per group) were weighed (weight: W_0) and placed in a six-well plate. Next, 2 mL PBS was added to each well to immerse the scaffolds, before placing the plate on a shaker in a 37 ℃ incubator. Following incubation, the scaffolds were washed with double distilled water and

then weighed after vacuum-drying at 50 °C (weight: W). The following equation was used to calculate degradation rates: in vitro degradation rate=$(W_0-W)/W_0\times100\%$.

2.3 Subcutaneous implantation of scaffolds in rats

The Shanghai Slac Laboratory (Shanghai, China) provided the specific-pathogen-free Sprague-Dawley (SD) rats. All 24 rats (12 for each group) were subjected to 3% (0.03 g/mL) sodium pentobarbital (Sigma-Aldrich) anesthesia, followed by hair removal on the back before surgery. After routine disinfection of the operation site, skin incisions were made parallel to the spine, about 2 cm from the spine, one on each side, followed by subcutaneous implantation of an NAg-CCS (one on one side and the blank CCS on the other side). The incision site was then sterilized, sutured, dressed, and bandaged with compression bandages. The movements of the rats were not affected. Rats in different groups were euthanized on postoperative Days 3 and 7. Implants were harvested by cutting the skin along the midline of the back for photographing and subsequent biological experiments. The detailed procedures of rat experiments are presented in Fig. S1.

2.4 Wound transplantation of scaffolds in miniature pigs

Twelve female miniature pigs (each about 15 kg in weight) purchased from Wuxi Hengtai Experimental Animal Farm (Wuxi, China) were used in this experiment. A dose of 1.0 mL/kg of 3% sodium pentobarbital was used for anesthesia and maintained at 0.5 mL/kg during the surgery. Each pig's back was shaved and six circular 2.0 cm-diameter full-thickness wounds were created (three on each side, symmetrically placed) (Fig. S2). This was followed by placing the NAg-CCSs on the right side wounds and blank CCSs on the left side wounds and suturing the scaffolds with the surrounding normal tissues with absorbable sutures. Following transplantation, the wounds were sterilized with 2.5% (0.025 g/mL) povidone-iodine solution, compression bandages were applied, and the animals were raised in individual cages. The pigs were monitored daily, and the surgical dressing was changed every other day until the wounds healed. On postoperative Days 7, 10, 14, 21, 28, and 60, the pigs were anesthetized to photograph the wounds. At each time point, two pigs were operated on to collect the wound samples, which were fixed in 4% (volume fraction) paraformaldehyde or placed in liquid nitrogen (subsequently at −80 °C for long-term storage) for later experiments, and then euthanized with excessive sodium pentobarbital. The detailed procedures of rat experiments are presented in Fig. S2.

2.5 Histological analysis

For histological analysis, paraformaldehyde-fixed samples were dehydrated with ethanol in a graded series, embedded in paraffin, and sectioned. The results of skin sections were observed and photographed after hematoxylin-eosin (HE) staining and Masson's trichrome staining according to standard procedures.

2.6 Immunohistochemistry

For immunohistochemistry (IHC) analysis, deparaffinized tissue sections were washed three times in PBS before being blocked for 30 min with 5% (0.05 g/mL) serum (Sigma, USA). Following blocking, the rat tissue sections were incubated with rabbit anti-tissue inhibitor of metalloproteinase-1 (TIMP-1) primary antibody (1:200 (volume ratio, the same below; Abcam, USA) and rabbit anti-matrix metalloproteinase-1 (MMP-1) primary antibody (1:200; Abcam). The sections were further incubated with the secondary antibody (1:500; Abcam) for 30 min at room temperature, washed three times in PBS, and counterstained with diaminobenzidine solution and hematoxylin. The average optical density (AOD) was measured using ImageJ 1.53q software (NIH, USA), with AOD=integrated optical density (IOD)/area.

2.7 Immunofluorescence

For immunofluorescence (IF) staining, sections were subjected to antigen retrieval following deparaffinization in xylene solutions and dehydration in graded ethanol solutions. The sections were rinsed with 0.01 mol/L PBS with Tween-20 (PBST) three times (5 min each), followed by blocking with the goat serum for 30 min at room temperature. After removing the excess liquid on the sections using absorbent paper, a drop of primary antibody mixture (25 μL) containing rabbit anti-interleukin (IL)-6 and mouse anti-IL10 antibodies (1:100; Abcam) was added to each slide, and then the sections were incubated in a moisture chamber at 4 °C overnight. The next day, the sections were washed with PBS after warming in a 37 °C incubator and incubated with 25 μL fluorescent secondary

antibodies (Alexa Fluor 488-conjugated AffiniPure goat anti-rabbit immunoglobulin G (IgG) and Alexa Fluor 594-conjugated AffiniPure goat anti-mouse IgG, 1:1000; Jackson ImmunoResearch, USA) in a moist dark chamber for 90 min at room temperature. After three washes in PBS, 4',6-diamidino-2-phenylindole (DAPI)-containing anti-fade mounting medium was used to mount the slides before observing them under a fluorescence microscope. The number of IF-positively stained cells was counted from four randomly selected high-magnification images (200×) using ImageJ software.

2.8 RNA isolation and qRT-PCR

RNA was extracted from skin tissues using a MolPure® TRIezay Plus Total RNA kit (Yeasen, Shanghai, China), and the concentration and purity were determined using a DS-11 spectrophotometer (DeNovix, Wilmington, DE, USA). The purified RNA was reverse-transcribed using a reverse transcription kit (TaKaRa, Kyoto, Japan) and the resulting products were subjected to quantitative real-time polymerase chain reaction (qRT-PCR) using a fluorescence quantification kit (TaKaRa) and the corresponding primers.

For qRT-PCR, the primers were designed and synthesized by Sangon Biotech (Shanghai, China), including rat *IL-6*, *IL-10*, and glyceraldehyde-3-phosphate dehydrogenase (*GAPDH*) (as the internal reference) for the rats (Table S1) and pig *collagen I*, *collagen III*, cluster of differentiation 68 (*CD68*), *CD163*, inducible nitric oxide synthase (*iNOS*), interferon-γ (*IFN-*γ), *IL-6*, *arginase-I*, major histocompatibility complex-II (*MHC-II*), resistin-like molecule alpha 1 (*FIZZ-1*), and *18S* (as the internal reference) for the pigs (Table S2). The PrimeScript™ RT Reagent Kit with gDNA Eraser and TB Green® Premix Ex Taq™ II (TaKaRa) was subsequently used for qRT-PCR. The results of qRT-PCR are presented based on the ΔC_T method ($\Delta C_T = C_{T,\text{target gene}} - C_{T,GAPDH/18S}$), using $2^{\Delta C_T} \times 10^6$ to indicate the relative gene expression level.

2.9 Protein isolation and western blot analysis

For western blotting, the frozen tissue samples were placed in radio immunoprecipitation assay (RIPA) lysis buffer containing phenylmethylsulfonyl fluoride and phosphatase inhibitor (Thermo Fisher Scientific) for complete lysis for 30 min, and then centrifuged at 13 000 r/min at 4 °C for 30 min to collect the supernatant. The extracted total protein in the supernatant was quantified using bicinchoninic acid assay (Thermo Fisher Scientific), and then 5× loading buffer was added to the protein samples which were then boiled for 10 min. After separating the protein samples on protein gels by electrophoresis (Bio-Rad Laboratory, USA), the separated proteins were transferred onto polyvinylidene fluoride (PVDF) membranes (Millipore, USA). The membranes were then blocked in 5% (0.05 g/mL) skimmed milk solution for 1 h and separately incubated with primary antibodies at 4 °C overnight. The membranes were washed three times in PBST (5 min each) after incubation and then immersed in the secondary antibodies at room temperature for 1.5 h. Proteins were detected using Pierce ECL western blotting substrate (Thermo Fisher Scientific) after washing in Tris-buffered saline with Tween-20 (TBST) three times (5 min each). The primary antibodies used included rabbit anti-collagen I, rabbit anti-collagen III, rabbit anti-CD68, rabbit anti-CD163, rabbit anti-iNOS, rabbit anti-IFN-γ, rabbit anti-arginase-I, rabbit anti-FIZZ-1, mouse anti-IL-6, mouse anti-MHC-II, and rabbit anti-β-actin (all from Abcam). The target proteins were quantitatively standardized with the internal reference using ImageJ software: normalized expression=grey value of the target protein/grey value of β-actin.

2.10 Statistical analysis and figure preparation

All quantitative data were analyzed and graphed using Origin 2019b software (OriginLab Corporation, USA), and are presented as the mean±standard deviation (SD). Differences between specimens were assessed using Student's *t*-test or analysis of variance (ANOVA). *P*-values of <0.05 were considered statistically significant. ImageJ 1.53q (National Institutes of Health, USA) was used for image processing and analysis, and Adobe Illustrator CC 2018 (Adobe Inc., USA) was used for processing and typesetting of results.

3 Results

3.1 Construction and characterization of NAg-CCS

The NAg-CCSs were prepared by a freeze-drying method (Fig. 1a). They were slightly yellow, with hollow and sponge-like structures inside the scaffold. The distribution of NAg in the internal structure of the scaffolds was observed under an electron microscope. The NAg was evenly distributed and tightly combined

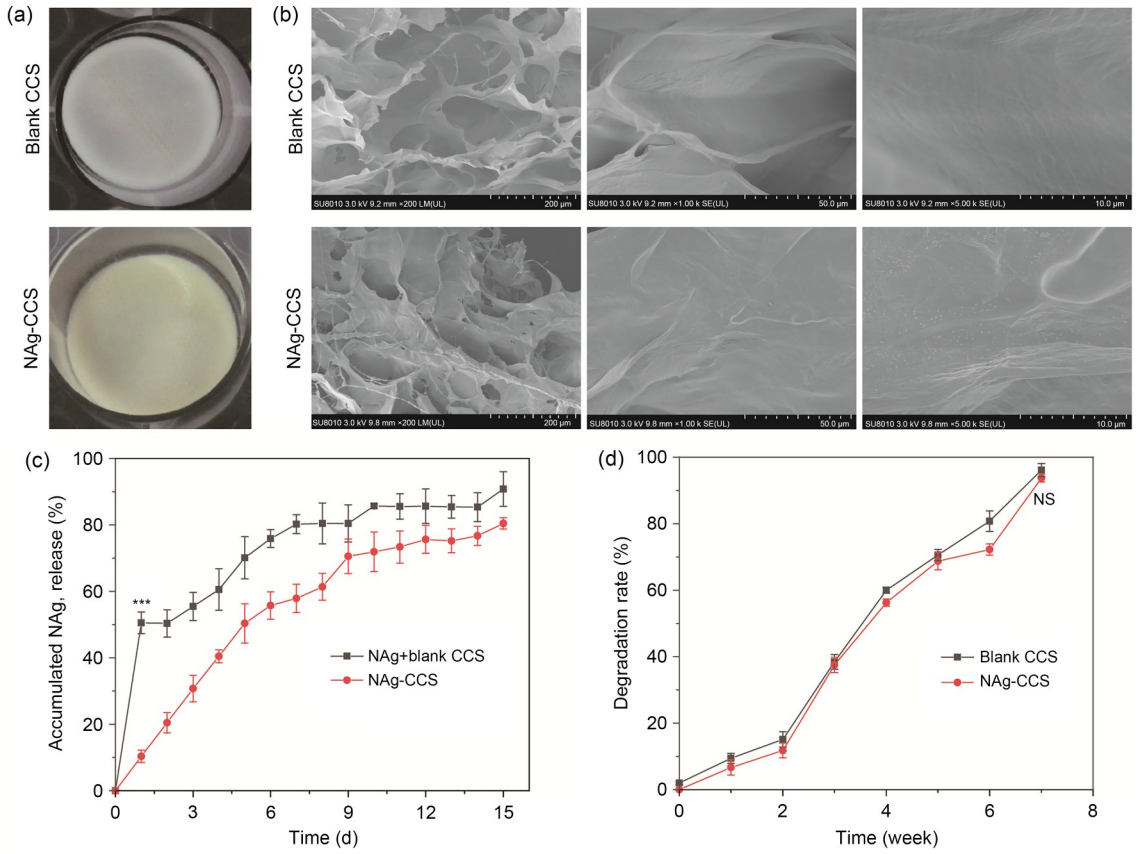

Fig. 1 Characteristic portraits of scaffolds. (a) Gross observation of blank CCS and NAg-CCS in a 24-well plate. (b) Microstructures of blank CCS and NAg-CCS under scanning electron microscopy with three different magnifications. (c) Cumulative release of NAg within two weeks; the mixed NAg in blank CCS exhibited a sudden release on Day 1, while a slow and sustained release of NAg was observed in the NAg-CCS group ((50.55±3.29)% vs. (10.34±1.88)%, *** P<0.001). (d) Degradation rates of blank CCS and NAg-CCS, with no significance (NS) in Week 7 ((96.15±2.04)% vs. (93.75±1.23)%, P>0.05). Data are expressed as mean±standard deviation (SD), n=3. NAg: nanosilver; CCS: collagen-chitosan scaffold.

with the collagen (Fig. 1b). The release study revealed that the blank CCS with a mixture of NAg released 50% of NAg on Day 2, while no sudden release was observed in the NAg-CCS group (Fig. 1c). The NAg-CCS group showed a slow release of NAg within two weeks, and the cumulative release of NAg was (80.45±1.70)%, which was slightly lower than that of the blank CCS group ((90.78±5.21)%). Subsequent degradation experiments showed that the degradation rate of the scaffolds was not significantly altered after nanoparticle encapsulation (Fig. 1d).

3.2 Subcutaneous implantation of scaffolds in rats

In the NAg-CCS group, no foreign body reaction was observed around the scaffolds (Fig. 2a, top panels, for representative images). HE-staining revealed multinucleated giant cells that agglomerated in the blank CCS group and disorderly tissue growth. The NAg-CCS group had fewer multinucleated giant cells and the tissue grew in a more orderly manner (Fig. 2a, bottom panels). IHC showed that the blank CCS group had significantly higher tissue expression of MMP-1 and TIMP-1 (Figs. 2b–2d) than the NAg-CCS group.

3.3 IF staining of macrophages in subcutaneous implantation of rats

Double IF staining of IL-6 (green) and IL-10 (red) showed that the number of IL-6-positive cells (M1 macrophages) on Days 3 and 7 after scaffold implantation in the NAg-CCS group was much lower than that in the blank CCS group (Figs. 3a and 3b). However, the number of IL-10-positive cells (M2 macrophages) on Day 3 after scaffold implantation in the NAg-CCS group was not significantly different from that of the blank CCS group (Figs. 3a and 3c). On Day 7 after scaffold implantation, the number of IL-10-positive cells

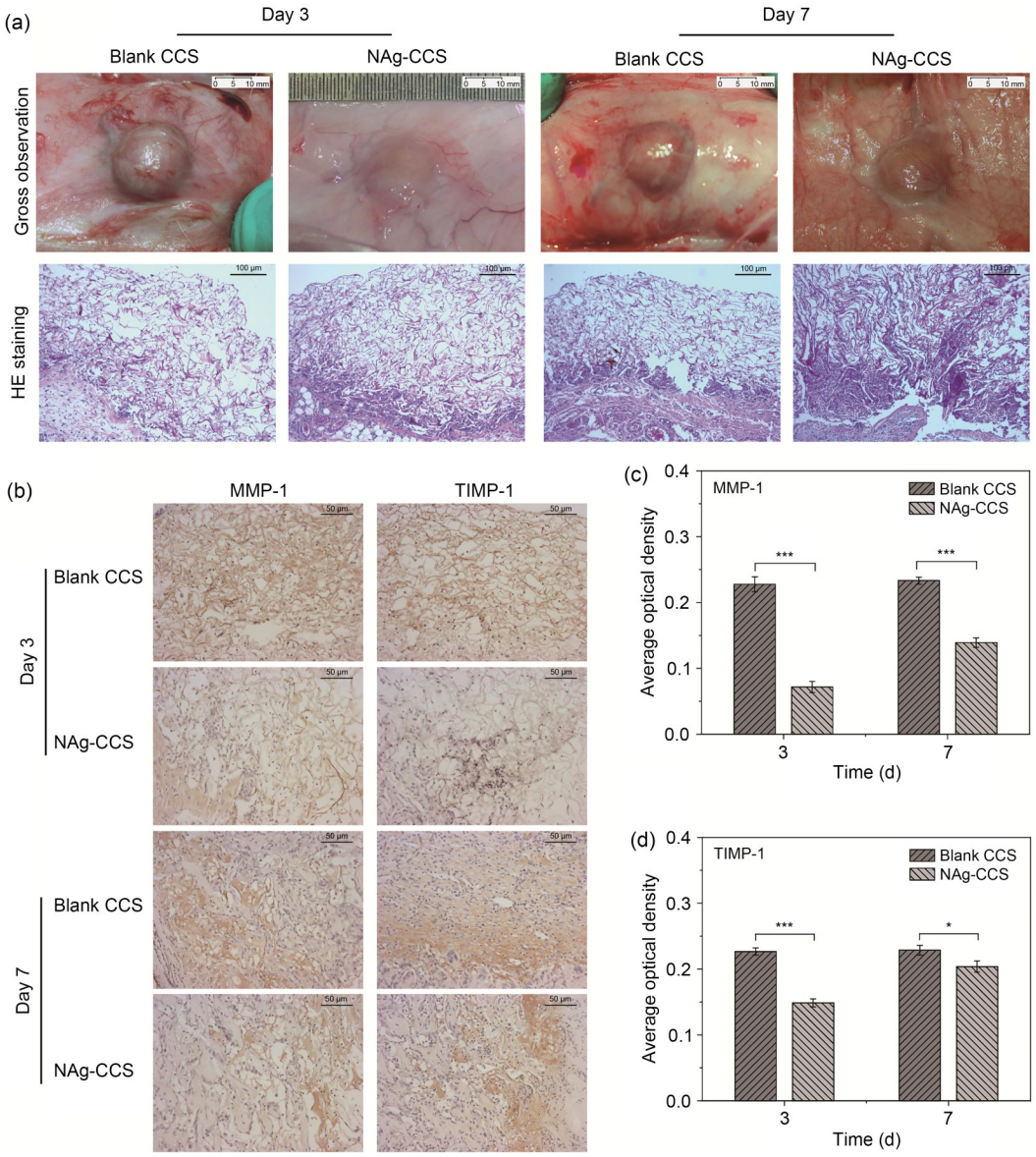

Fig. 2 Scaffold implantation in the back of rats. (a) Gross images (upper panels) and HE-stained (lower panels) back tissues of the NAg-CCS and blank CCS groups after scaffold implantation on postoperative Days 3 and 7. (b) Representative images showing the IHC of MMP-1 and TIMP-1 of the two groups. (c, d) Results of quantitative IHC analyses of MMP-1 (c) and TIMP-1 (d). Data are expressed as mean±standard deviation (SD) (n=3). * P<0.05, *** P<0.001. HE: hematoxylin-eosin; NAg: nanosilver; CCS: collagen-chitosan scaffold; IHC: immunohistochemistry; MMP-1: matrix metalloproteinase-1; TIMP-1: metallopeptidase inhibitor-1.

in the NAg-CCS group was significantly higher than that in the blank CCS group. The results of qRT-PCR showed that the expression of *IL-6* in the NAg-CCS group on both days was significantly inhibited compared with that in the blank CCS group (Fig. 3d). In contrast, the expression of *IL-10* in the NAg-CCS group on both days after scaffold implantation was significantly higher than that of the blank CCS group (Fig. 3e).

3.4 Wound repair experiment in miniature pigs

Fig. 4a shows the gross images of the back wounds of miniature pigs on postoperative Days 7, 14, 21, 28, and 60. They show that the wound healing of the NAg-CCS group was faster and better than that of the blank CCS group (Fig. 4b). On postoperative Day 7, the wound of the NAg-CCS group was red and moist, while the wound and blank CCS failed to combine

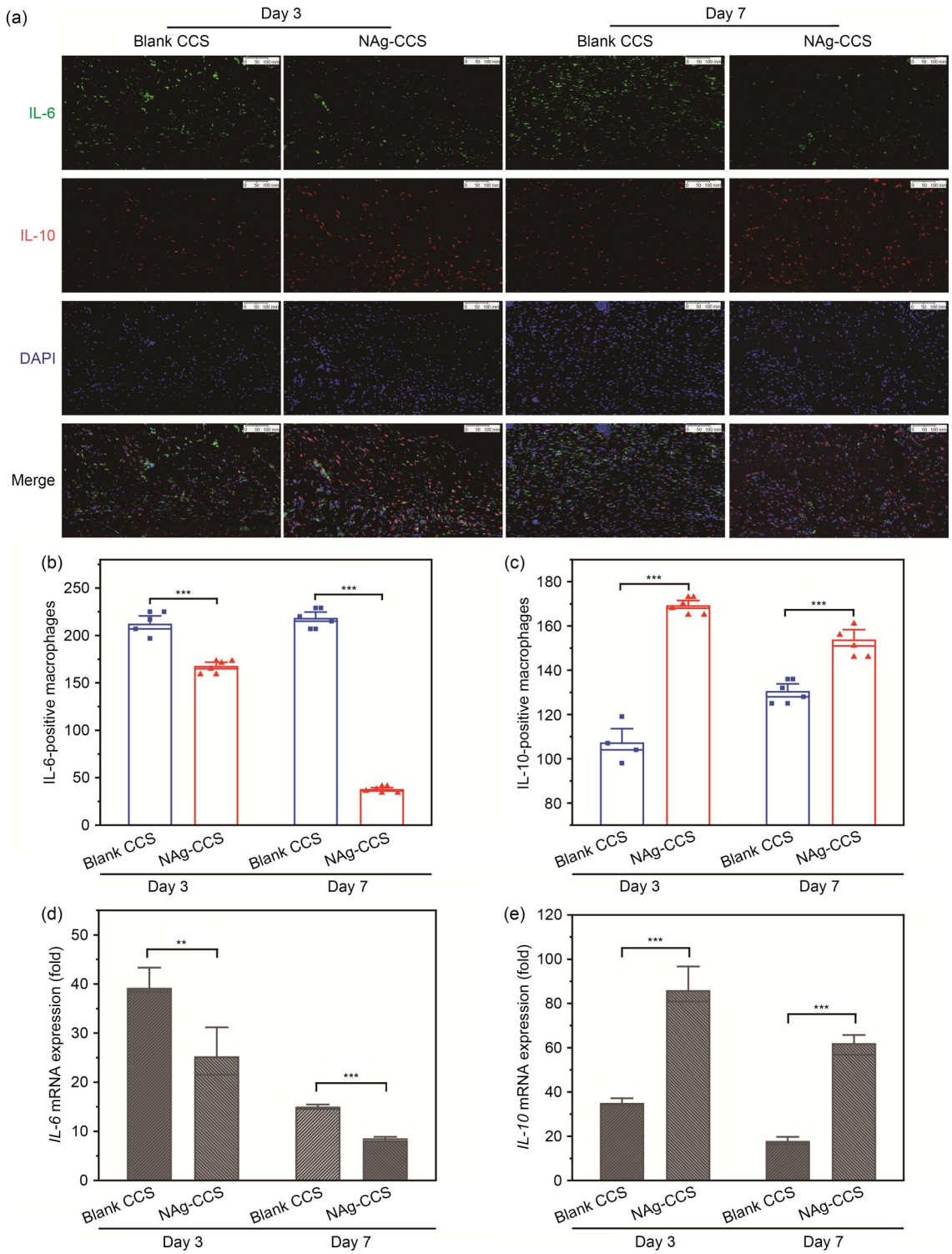

Fig. 3 IF and qRT-PCR results of IL-6 and IL-10 in the rats after scaffold implantation. (a) Representative images of IL-6 (green) and IL-10 (red) IF staining in the NAg-CCS and blank CCS groups on postoperative Days 3 and 7. (b, c) Cell counts of IL-6-positive (b) and IL-10-positive (c) macrophages in the NAg-CCS and blank CCS groups on Days 3 and 7 (n=4). (d, e) Relative mRNA expression of *IL-6* (d) and *IL-10* (e) detected by qRT-PCR in the NAg-CCS and blank CCS groups on Days 3 and 7 (n=3). Data are expressed as mean±standard deviation (SD). ** P<0.01, *** P<0.001. IF: immunofluorescence; qRT-PCR: quantitative real-time polymerase chain reaction; IL: interleukin; NAg: nanosilver; CCS: collagen-chitosan scaffold; mRNA: messenger RNA; DAPI: 4',6-diamidino-2-phenylindole.

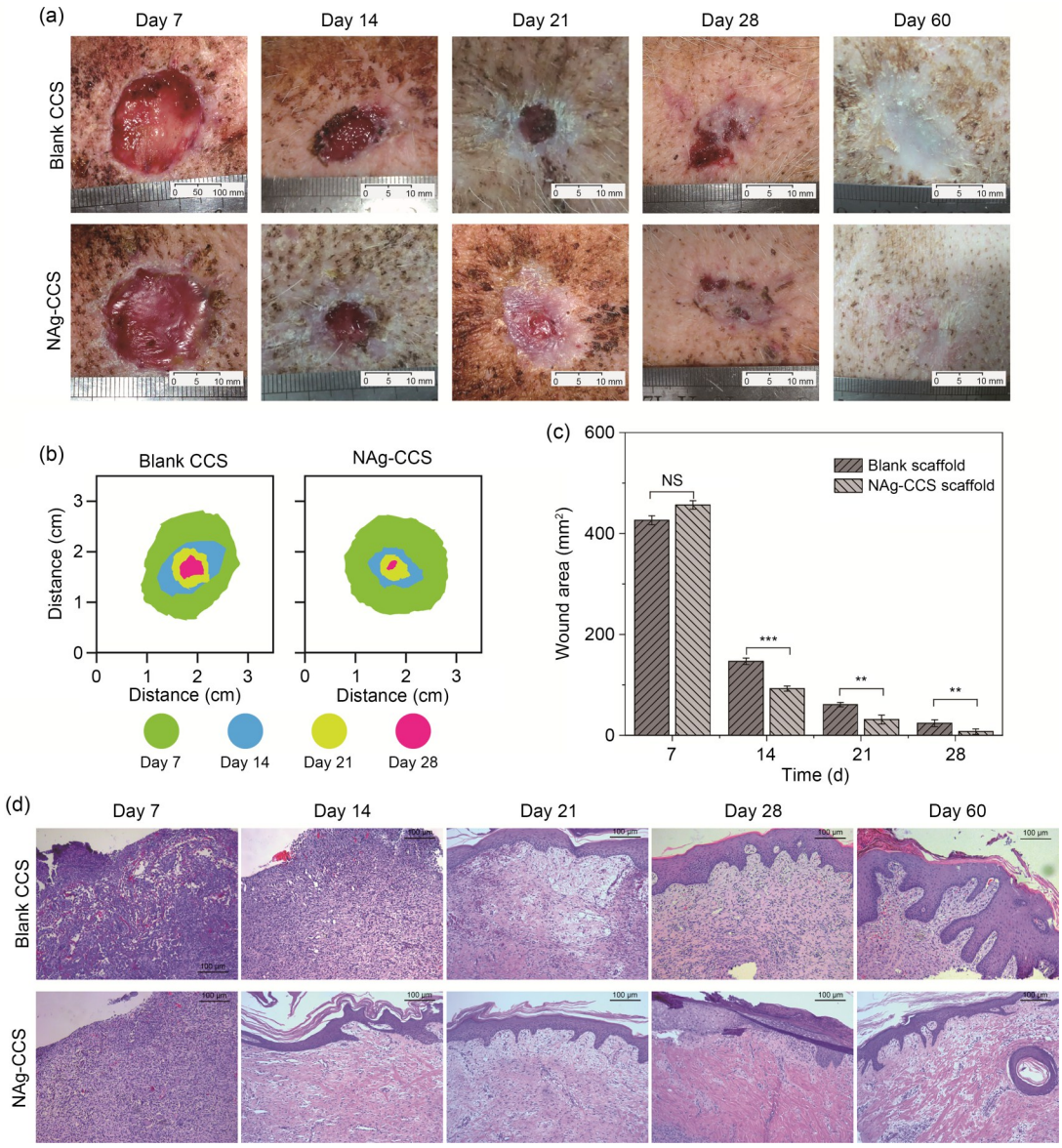

Fig. 4 Skin wound healing in miniature pigs. (a) Images show a gross view of the back tissues of miniature pigs in the blank CCS (upper panels) and NAg-CCS (lower panels) groups after scaffold implantation on postoperative Days 7, 14, 21, 28, and 60. (b) Overlaid images of the wound areas. (c) Quantitative analysis of wound areas. Data are expressed as mean±standard deviation (SD) (n=3). ** P<0.01, *** P<0.001; NS: not significant. (d) HE-staining results at different time points. NAg: nanosilver; CCS: collagen-chitosan scaffold; HE: hematoxylin-eosin.

tightly in the blank CCS group, with little substantial neovascularization on the wound base. On postoperative Day 14 onward, a significant difference in the rate of wound healing was found between the two groups: the NAg-CCS group had significantly smaller wounds than the blank CCS group. On postoperative Day 28, the NAg-CCS group had a more prominent epithelization and healing rate. Calculation of the wound area at different time points after implantation confirmed that the wound healing rate of the NAg-CCS group was significantly faster than that of the blank CCS group (Fig. 4c). HE staining (Fig. 4d) showed that on Day 7, the scaffolds of the NAg-CCS group had been replaced by new granulation tissues, while the residual scaffolds in the blank CCS group were easily distinguishable from the surrounding tissues, showing hyperemia, loose tissues, and gaps. Both groups showed numerous inflammatory cells, such as monocytes, which infiltrated the scaffold at an early stage. The inflammatory cells of the NAg-CCS group were gathered near the

base of the scaffold, while those of the blank CCS group had infiltrated the full layer of the scaffold, nearly reaching the surface. On postoperative Day 14, inflammation in the blank-CCS group was still pronounced, without showing evident epithelialization; in contrast, the infiltration of inflammatory cells in the NAg-CCS group was significantly reduced compared with that on postoperative Day 7. A single layer of epidermal cells had formed on the wound surface in the NAg-CCS group. Additionally, the NAg-CCS group had stratified epithelial cells on postoperative Day 21. On postoperative Day 60, the skin repaired by the NAg-CCS had an epidermis and dermis, with mature and complete skin appendages; in contrast, the blank CCS group had a disordered skin tissue structure.

3.5 Evaluation of collagen synthesis and deposition during wound healing

Evaluation of collagen regeneration showed that the blank CCS group had an uneven collagen distribution, showing as clumps or bundles in the later stage (Fig. 5a, upper panels). The collagen regeneration of the NAg-CCS group was stable and orderly, and collagen distribution was uniform (Fig. 5a, lower panels). In the

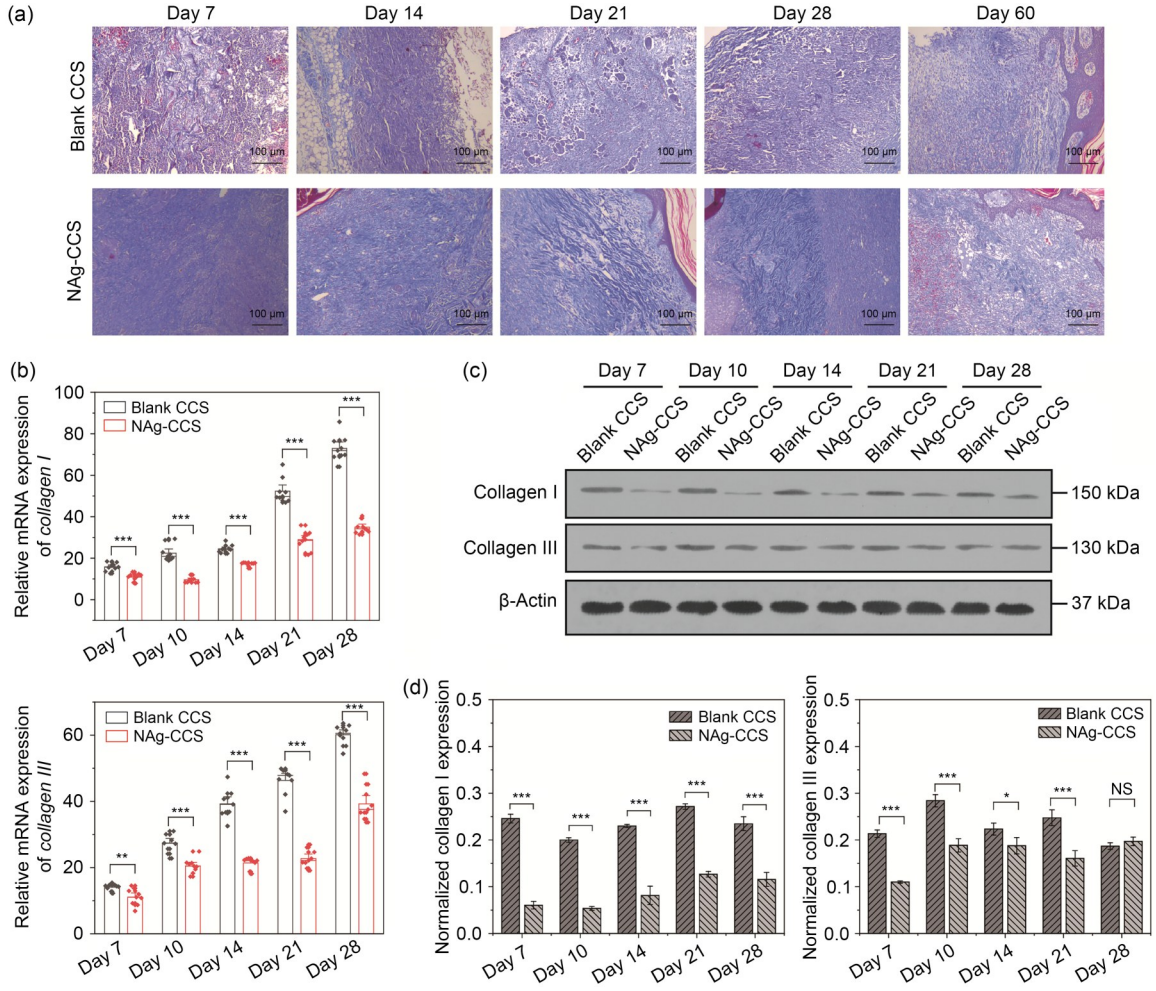

Fig. 5 Evaluation of collagen synthesis and deposition in miniature pigs following scaffold implantation. (a) Masson's trichrome staining of the back skin tissues of miniature pigs in the blank CCS (upper panels) and NAg-CCS (lower panels) groups after scaffold implantation on postoperative Days 7, 14, 21, 28, and 60. (b) The mRNA expression levels of *collagen I* (upper panel) and *collagen III* (lower panel) detected by qRT-PCR. (c) Representative images of western blotting showing the protein expression of collagen I and collagen III in the two groups at different postoperative time points. (d) Relative protein expression (western blotting) of collagen I and collagen III in different groups at different postoperative time points. Data are expressed as mean±standard deviation (SD) (n=3). * P<0.05, ** P<0.01, *** P<0.001; NS: not significant. NAg: nanosilver; CCS: collagen-chitosan scaffold; mRNA: messenger RNA; qRT-PCR: quantitative real-time polymerase chain reaction.

early stage, the regenerated dermis of the two groups was thin; the blank CCS group still had a visible undegraded scaffold, which was blue-gray and was surrounded by many inflammatory cells and blood cells. In the NAg-CCS group, the scaffold structure was degraded, and there was a flocculent secretion of new collagen at the base on postoperative Day 7. On postoperative Day 14, the blank CCS group still had degraded collagen particles, and the newly formed collagen was disordered. In contrast, the newly formed collagen in the NAg-CCS group was staggered, and the inflammatory response of the NAg-CCS group was gradually reducing. By the third week after implantation, the collagen deposition of the NAg-CCS group was reduced, while the blank CCS group still had numerous collagen depositions, showing as globular forms. On postoperative Day 28, unidirectional distribution of collagen in bundles was observed in the blank CCS group, while the collagen in the NAg-CCS group was distributed in a staggered pattern.

The results of qRT-PCR (Fig. 5b) showed that the overall transcript levels of collagen types I and III increased with time. The mRNA expression levels of collagen types I and III at different postoperative time points in the NAg-CCS group were lower than those in the blank CCS group. The results of western blotting showed that the protein level of collagen I in the NAg-CCS group was always lower than that in the blank CCS group at different postoperative time points, while collagen III was reduced at most time points except for Day 28 (Figs. 5c and 5d).

3.6 Evaluation of inflammation and macrophage infiltration in the miniature pig model

Further detection of differentiation and infiltration of macrophages in the wounds at different postoperative time points was performed using qRT-PCR. The results showed that the expression of *CD163* in the wounds of the NAg-CCS group was significantly higher, but the expression of *CD68* significantly lower, than that in the blank CCS group (Fig. 6a). In addition, western blotting revealed that CD163 expression was dominant in the NAg-CCS group only during the first two weeks, while CD68 expression was always higher in the blank CCS group (Figs. 6b and 6c). Moreover, in the early and intermediate stages of wound tissue repair (postoperative Days 7, 10, 14, and 21), the mRNA expression of proinflammatory cytokines *iNOS*, *IL-6*, and *IFN-γ* of the NAg-CCS group was significantly reduced, while that of anti-inflammatory cytokines, including *arginase-I*, *MHC-II*, and *FIZZ-1*, was significantly increased in the NAg-CCS group (Fig. 6d). Similar findings from western blotting confirmed the differences in proinflammatory and anti-inflammatory cytokine expression (Figs. 6e and 6f).

4 Discussion

Our research demonstrated that NAg-CCS had good biocompatibility and was able to reduce inflammation and induce macrophage differentiation. Subcutaneous implantation studies in rats and skin transplantation studies in miniature pigs confirmed that NAg can activate macrophage conversion and ameliorate the inflammatory microenvironment, thereby suppressing the foreign body reaction and inducing regeneration and in situ repair of skin wounds.

We used CD68 as a marker of M1 macrophages and CD163 as a specific surface molecular marker for M2 macrophages. The relative quantification of CD68 and CD163 proteins roughly distinguishes the activation of M1 and M2 macrophages (Vannella and Wynn, 2017; Huang et al., 2018; Kim et al., 2019). The results showed that M1 macrophages in the wound tissues of the NAg-CCS group were significantly lower than that of the blank CCS group, while M2 macrophage aggravation in the NAg-CCS group was more abundant. This indicated that NAg ameliorated the foreign body reaction after scaffold implantation and reduced the infiltration of giant cells and inflammatory cells around the scaffolds in the early stage. Besides, overactive M1 macrophages can also activate M2 macrophages intensively, resulting in a subsequent proliferation of fibrous tissues surrounding the scaffold and aggravating the formation of foreign body granulomas (Anderson et al., 2008; Witherel et al., 2021). Therefore, an orderly transition from the inflammatory phase to the recovery phase is critical for extending the retention of implanted scaffolds. Our results showed that wounds repaired by scaffolds without NAg had more M1 macrophage aggregation in the early and middle stages. In contrast, scaffolds containing NAg effectively controlled the inflammation and induced M2 macrophage activation at the early stage to initiate wound repair and accelerate orderly wound healing (Seo et al., 2012; You et al.,

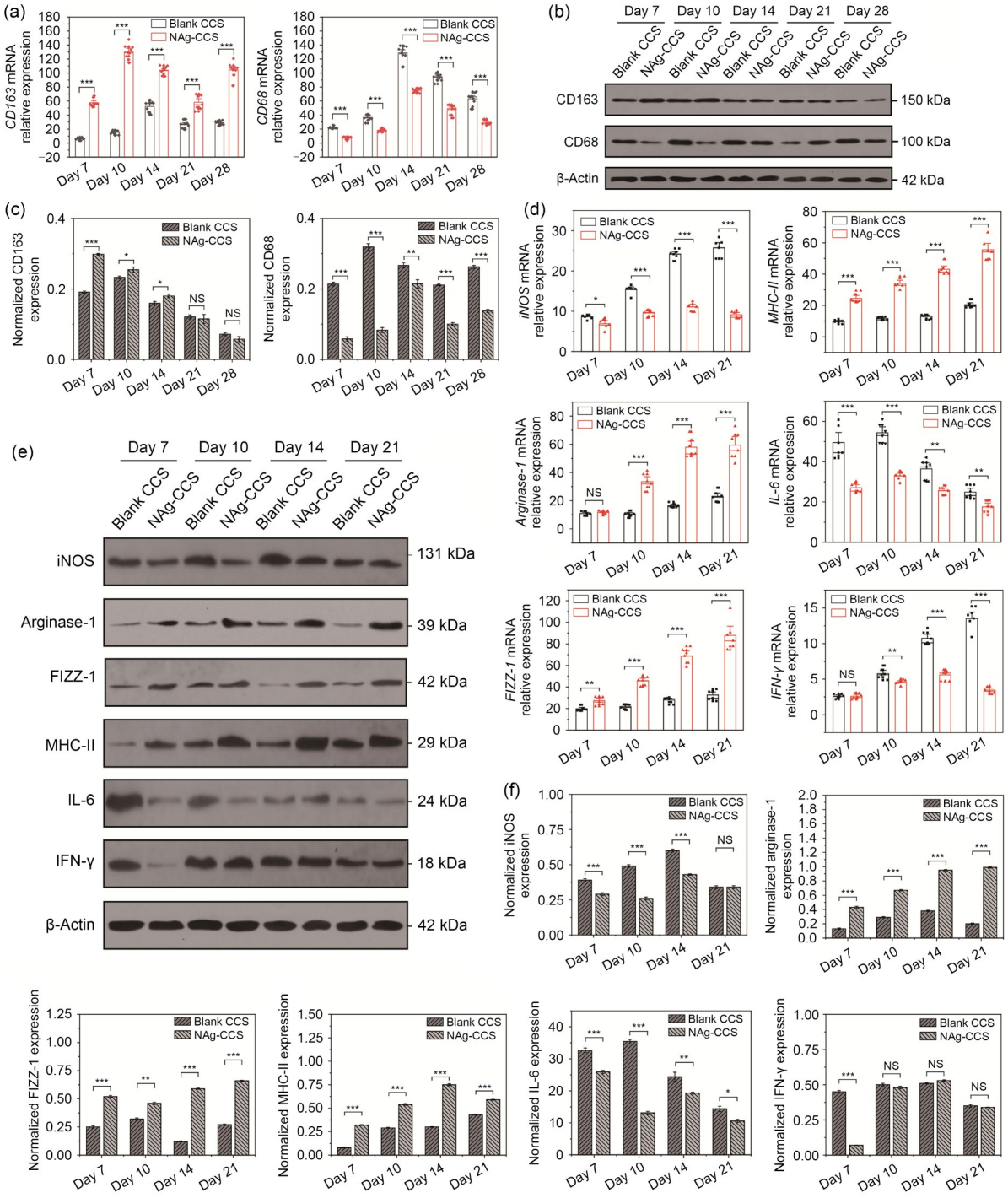

Fig. 6 Inflammation and macrophage infiltration after scaffold implantation in miniature pigs. (a) Relative mRNA expression of *CD163* (left panel) and *CD68* (right panel) was detected by qRT-PCR. (b) Representative images showing results for western blotting of CD163 and CD68. (c) Relative protein expression of CD163 (left panel) and CD68 (right panel). (d) Relative mRNA expression of *iNOS*, *arginase-1*, *FIZZ-1*, *MHC-II*, *IL-6*, and *IFN-γ*. (e) Representative images showing the western blotting results of iNOS, arginase-1, FIZZ-1, MHC-II, IL-6, and IFN-γ. (f) Relative protein expression of iNOS, arginase-1, FIZZ-1, MHC-II, IL-6, and IFN-γ. Data are expressed as mean±standard deviation (SD) (n=3). * P<0.05, ** P<0.01, *** P<0.001; NS: not significant. NAg: nanosilver; CCS: collagen-chitosan scaffold; mRNA: messenger RNA; CD: cluster of differentiation; qRT-PCR: quantitative real-time polymerase chain reaction; iNOS: inducible nitric oxide synthase; FIZZ-1: resistin-like molecule alpha 1; MHC-II: major histocompatibility complex-II; IL-6: interleukin-6; IFN-γ: interferon-γ.

2017; Alsaleh et al., 2019). Hence, in the absence of NAg, long-term abnormal inflammation of the wound tissue may occur resulting in granulomas, infection, or necrosis, eventually leading to the failure of tissue repair (Chu et al., 2020; Witherel et al., 2021).

M1 and M2 macrophages also play coordinating roles in the wound healing process by secreting cytokines, such as IL-6, transforming growth factor-β (TGF-β), tumor necrosis factor-α (TNF-α), and IL-8, to mobilize peripheral or systemic monocytes and lymphocytes to gather around the wound surface (Snyder et al., 2016; Wynn and Vannella, 2016). Therefore, we analyzed different macrophage activation-related proteins, such as iNOS, IFN-γ, and IL-6 as the markers for activated M1 macrophages, and arginase-I, MHC-II, and FIZZ-1 as markers for activated M2 macrophages, to further evaluate the dynamic activation of macrophages at different time points after scaffold implantation. iNOS is an intermediate metabolite of activated M1 macrophages involved in antibacterial-related biological processes (Orecchioni et al., 2019; Paul et al., 2019). IFN-γ and TNF-α induce activation of Ml macrophages to trigger a respiratory burst, release reactive oxygen species, secrete TNF-α and IL-12, induce iNOS, and upregulate expression of programmed death-ligand 1 (PD-L1) (Jain and Vogel, 2018; Tan et al., 2019). M2 macrophages are induced by IL-4 and IL-13 to upregulate IL-10 and FIZZ-1 and secrete less IL-12 and nitric oxide, weakening the phagocytosis of pathogenic microorganisms (Locati et al., 2020; Yunna et al., 2020; Witherel et al., 2021). The results of qRT-PCR and western blotting showed that the mRNA expression of M1 macrophage markers, *iNOS*, *IFN-γ*, and *IL-6*, was high in the blank-CCS group, while that of M2 macrophage markers, *arginase-I*, *MHC-II*, and *FIZZ-1* was high in the NAg-CCS group.

In addition, the mechanism by which NAg regulates macrophage polarization is probably related to its antimicrobial properties. In previous studies, we demonstrated that NAg has a strong anti-infection effect and can significantly inhibit the expression of inflammatory factors, most of which are secreted by macrophages (You et al., 2012, 2017). It could be assumed that the mechanisms of NAg involved in promoting healing might be closely connected to its anti-inflammatory and analgesic effects, though further experiments are needed to confirm significant connections between the antimicrobial effects and macrophage conversion. These results further support the notion that NAg regulates macrophage polarization and the expression of related cytokines, thereby playing a positive role in the process of skin wound healing.

We used Masson's trichrome staining to evaluate the repair quality of the dermal tissues near the scaffolds. Results showed that the contents of collagen types I and III in the dermal tissues of the NAg-CCS group were lower than those in the blank-CCS group (Fig. 6b). Additionally, the inflammatory response of the NAg-CCS group was gradually alleviated, and the newly formed collagen in the NAg-CCS group was staggered, almost resembling normal skin on postoperative Days 21 and 28. These results indicated that NAg-CCS inhibited the inflammatory response to foreign bodies and promoted high-quality tissue repair (You et al., 2017). qRT-PCR and western blotting showed that the secretion and expression of the two collagens in the NAg-CCS group were less than those of the blank CCS group, which confirmed the previous hypothesis. M1 macrophages secrete numerous proteolytic enzymes to degrade extracellular matrix (ECM), including collagens, elastin, and fibronectin. M2 macrophages secrete ECM cross-linking enzymes, such as glutaminyl transferase and osteopontin, which promote ECM and cell adhesion, suggesting that both macrophages play important roles in collagen deposition (Wynn and Vannella, 2016; Hesketh et al., 2017; Liu et al., 2021). Previous studies have shown that fibroblasts cocultured with M1 macrophages have reduced collagen synthesis and proliferation, whereas those cocultured with M2 macrophages have increased collagen synthesis and proliferation (Gomes et al., 2021; Li and Cui, 2021; Motz et al., 2021). Activation of M2 macrophages at an earlier stage led to faster matrix synthesis and deposition around the implant (Li and Cui, 2021; Furtado et al., 2022), reduced the foreign body reaction caused by inflammatory activation, and enabled the healing process to shift from the inflammatory phase to the proliferative phase more quickly, achieving complete wound healing and reducing scar formation.

5 Conclusions

NAg-CCS successfully alleviates foreign body reactions and inflammation around implants and promotes wound repair by suppressing M1 macrophage

activation and inflammatory cytokine secretion. Also, NAg accelerates transition of the repair process from the inflammatory phase to the proliferation phase by regulating M2 macrophage conversion, thereby facilitating the deposition of ECM and promoting high-quality wound healing.

Acknowledgments

This work was supported by the Zhejiang Province Key Research and Development Program (No. 2019C03083), the Zhejiang Provincial Basic Public Welfare Research Program (No. LGF19H150008), and the National Natural Science Foundation of China (Nos. 81601681 and 81871558).

Author contributions

Conceptualization and methodology: Chuangang YOU and Zhikang ZHU; Formal analysis: Shuangshuang WANG, Xingang WANG, and Chuangang YOU; Funding acquisition: Huawei SHAO, Zhikang ZHU, Chuangang YOU, and Chunmao HAN; Supervision: Chunmao HAN and Huawei SHAO; Writing – original draft: Chuangang YOU and Zhikang ZHU; Writing – review and editing: Chunmao HAN and Huawei SHAO. All authors have read and approved the final manuscript, and therefore, have full access to all the data in the study and take responsibility for the integrity and security of the data.

Compliance with ethics guidelines

Chuangang YOU, Zhikang ZHU, Shuangshuang WANG, Xingang WANG, Chunmao HAN, and Huawei SHAO disclose that there is no financial and personal relationship with other people or organizations that might raise any questions of bias in our work.

Experiments were approved and supervised by the Animal Care and Ethical Committee of the Second Affiliated Hospital of Zhejiang University (No. 2020-720).

References

Alsaleh NB, Minarchick VC, Mendoza RP, et al., 2019. Silver nanoparticle immunomodulatory potential in absence of direct cytotoxicity in RAW 264.7 macrophages and MPRO 2.1 neutrophils. *J Immunotoxicol*, 16(1):63-73. https://doi.org/10.1080/1547691x.2019.1588928

Anderson JM, Jiang SR, 2017. Implications of the acute and chronic inflammatory response and the foreign body reaction to the immune response of implanted biomaterials. *In*: Corradetti B (Ed.), The Immune Response to Implanted Materials and Devices: the Impact of the Immune System on the Success of an Implant. Springer, Cham, p.15-36. https://doi.org/10.1007/978-3-319-45433-7_2

Anderson JM, Rodriguez A, Chang DT, 2008. Foreign body reaction to biomaterials. *Semin Immunol*, 20(2):86-100. https://doi.org/10.1016/j.smim.2007.11.004

Benayahu D, Pomeraniec L, Shemesh S, et al., 2020. Biocompatibility of a marine collagen-based scaffold in vitro and in vivo. *Mar Drugs*, 18(8):420. https://doi.org/10.3390/md18080420

Bergan JJ, 2005. Chronic venous insufficiency and the therapeutic effects of Daflon 500 mg. *Angiology*, 56(6_suppl): S21-S24. https://doi.org/10.1177/00033197050560i104

Chiang YZ, Pierone G, Al-Niaimi F, 2017. Dermal fillers: pathophysiology, prevention and treatment of complications. *J Eur Acad Dermatol Venereol*, 31(3):405-413. https://doi.org/10.1111/jdv.13977

Chu CY, Liu L, Rung S, et al., 2020. Modulation of foreign body reaction and macrophage phenotypes concerning microenvironment. *J Biomed Mater Res Part A*, 108(1): 127-135. https://doi.org/10.1002/jbm.a.36798

Forbes JM, Cooper ME, 2013. Mechanisms of diabetic complications. *Physiol Rev*, 93(1):137-188. https://doi.org/10.1152/physrev.00045.2011

Furtado M, Chen L, Chen ZH, et al., 2022. Development of fish collagen in tissue regeneration and drug delivery. *Eng Regener*, 3(3):217-231. https://doi.org/10.1016/j.engreg.2022.05.002

Gomes A, Leite F, Ribeiro L, 2021. Adipocytes and macrophages secretomes coregulate catecholamine-synthesizing enzymes. *Int J Med Sci*, 18(3):582-592. https://doi.org/10.7150/ijms.52219

Hesketh M, Sahin KB, West ZE, et al., 2017. Macrophage phenotypes regulate scar formation and chronic wound healing. *Int J Mol Sci*, 18(7):1545. https://doi.org/10.3390/ijms18071545

Huang YJ, Hung KC, Hung HS, et al., 2018. Modulation of macrophage phenotype by biodegradable polyurethane nanoparticles: possible relation between macrophage polarization and immune response of nanoparticles. *ACS Appl Mater Interfaces*, 10(23):19436-19448. https://doi.org/10.1021/acsami.8b04718

Jain N, Vogel V, 2018. Spatial confinement downsizes the inflammatory response of macrophages. *Nat Mater*, 17(12): 1134-1144. https://doi.org/10.1038/s41563-018-0190-6

Kim H, Wang SY, Kwak G, et al., 2019. Exosome-guided phenotypic switch of M1 to M2 macrophages for cutaneous wound healing. *Adv Sci*, 6(20):1900513. https://doi.org/10.1002/advs.201900513

Li CD, Cui WG, 2021. 3D bioprinting of cell-laden constructs for regenerative medicine. *Eng Regener*, 2:195-205. https://doi.org/10.1016/j.engreg.2021.11.005

Liu C, Xu XY, Cui WG, et al., 2021. Metal-organic framework (MOF)-based biomaterials in bone tissue engineering. *Eng Regener*, 2:105-108. https://doi.org/10.1016/j.engreg.2021.09.001

Locati M, Curtale G, Mantovani A, 2020. Diversity, mechanisms, and significance of macrophage plasticity. *Annu Rev Pathol Mech Dis*, 15:123-147. https://doi.org/10.1146/annurev-pathmechdis-012418-012718

Motz K, Lina I, Murphy MK, et al., 2021. M2 macrophages promote collagen expression and synthesis in laryngotracheal stenosis fibroblasts. *Laryngoscope*, 131(2):E346-E353.

https://doi.org/10.1002/lary.28980

Orecchioni M, Ghosheh Y, Pramod AB, et al., 2019. Macrophage polarization: different gene signatures in M1(LPS+) vs. classically and M2(LPS−) vs. alternatively activated macrophages. *Front Immunol*, 10:1084. https://doi.org/10.3389/fimmu.2019.01084

O'Shea TM, Wollenberg AL, Kim JH, et al., 2020. Foreign body responses in mouse central nervous system mimic natural wound responses and alter biomaterial functions. *Nat Commun*, 11:6203. https://doi.org/10.1038/s41467-020-19906-3

Paul S, Chhatar S, Mishra A, et al., 2019. Natural killer T cell activation increases $iNOS^{+}CD206^{-}$ M1 macrophage and controls the growth of solid tumor. *J ImmunoTher Cancer*, 7(1):208. https://doi.org/10.1186/s40425-019-0697-7

Seo SY, Lee GH, Lee SG, et al., 2012. Alginate-based composite sponge containing silver nanoparticles synthesized in situ. *Carbohydr Polym*, 90(1):109-115. https://doi.org/10.1016/j.carbpol.2012.05.002

Sheikh Z, Brooks PJ, Barzilay O, et al., 2015. Macrophages, foreign body giant cells and their response to implantable biomaterials. *Materials*, 8(9):5671-5701. https://doi.org/10.3390/ma8095269

Shi CY, Wang CY, Liu H, et al., 2020. Selection of appropriate wound dressing for various wounds. *Front Bioeng Biotechnol*, 8:182. https://doi.org/10.3389/fbioe.2020.00182

Shi K, Qiu X, Zheng W, et al., 2018. MiR-203 regulates keloid fibroblast proliferation, invasion, and extracellular matrix expression by targeting EGR1 and FGF2. *Biomed Pharmacother*, 108:1282-1288. https://doi.org/10.1016/j.biopha.2018.09.152

Snyder RJ, Lantis J, Kirsner RS, et al., 2016. Macrophages: a review of their role in wound healing and their therapeutic use. *Wound Repair Regen*, 24(4):613-629. https://doi.org/10.1111/wrr.12444

Tan RZ, Liu J, Zhang YY, et al., 2019. Curcumin relieved cisplatin-induced kidney inflammation through inhibiting Mincle-maintained M1 macrophage phenotype. *Phytomedicine*, 52:284-294. https://doi.org/10.1016/j.phymed.2018.09.210

Vannella KM, Wynn TA, 2017. Mechanisms of organ injury and repair by macrophages. *Annu Rev Physiol*, 79:593-617. https://doi.org/10.1146/annurev-physiol-022516-034356

Villarreal-Leal RA, Healey GD, Corradetti B, 2021. Biomimetic immunomodulation strategies for effective tissue repair and restoration. *Adv Drug Deliv Rev*, 179:113913. https://doi.org/10.1016/j.addr.2021.113913

Weng TT, Wu P, Zhang W, et al., 2020. Regeneration of skin appendages and nerves: current status and further challenges. *J Transl Med*, 18:53. https://doi.org/10.1186/s12967-020-02248-5

Wicks K, Torbica T, Mace KA, 2014. Myeloid cell dysfunction and the pathogenesis of the diabetic chronic wound. *Semin Immunol*, 26(4):341-353. https://doi.org/10.1016/j.smim.2014.04.006

Witherel CE, Sao K, Brisson BK, et al., 2021. Regulation of extracellular matrix assembly and structure by hybrid M1/M2 macrophages. *Biomaterials*, 269:120667. https://doi.org/10.1016/j.biomaterials.2021.120667

Wynn TA, Vannella KM, 2016. Macrophages in tissue repair, regeneration, and fibrosis. *Immunity*, 44(3):450-462. https://doi.org/10.1016/j.immuni.2016.02.015

Yang YX, Zhao XD, Yu J, et al., 2021. Bioactive skin-mimicking hydrogel band-aids for diabetic wound healing and infectious skin incision treatment. *Bioact Mater*, 6(11):3962-3975. https://doi.org/10.1016/j.bioactmat.2021.04.007

You CG, Han CM, Wang XG, et al., 2012. The progress of silver nanoparticles in the antibacterial mechanism, clinical application and cytotoxicity. *Mol Biol Rep*, 39(9):9193-9201. https://doi.org/10.1007/s11033-012-1792-8

You CG, Li Q, Wang XG, et al., 2017. Silver nanoparticle loaded collagen/chitosan scaffolds promote wound healing via regulating fibroblast migration and macrophage activation. *Sci Rep*, 7:10489. https://doi.org/10.1038/s41598-017-10481-0

Yunna C, Mengru H, Lei W, et al., 2020. Macrophage M1/M2 polarization. *Eur J Pharmacol*, 877:173090. https://doi.org/10.1016/j.ejphar.2020.173090

Supplementary information

Figs. S1 and S2; Tables S1 and S2